Multi-focus Image Fusion Based on Guided Image Filtering

Ya-ting Yuan[1], Li Chen[1*], Yong-xin Zhang[2,1], Shan-shan Li[1]

[1] Department of Information Science and Technology, Northwest University, Xi'an 710127, Shaanxi, China
2669059710_yy@sina.com, chenli@nwu.edu.cn

[2] Department of Land and Tourism, Luoyang Normal University, Luoyang 471022, He'nan, China

Abstract. Image fusion is merged to form a single image, which is more informative than the single input image in quality and appearance. In order to represent the source images effectively and completely, a novel guided image filtering based fusion (GFF) for multi-focus images is proposed. Guided image filtering decomposes an image into a base layer and a detail layer. The base layer contains large scale variations in intensity and the detail layer captures small scale details. The focus region of the base layer is detected according to energy of image gradient (EOG). The focus region of the detail layer is detected using spatial frequency (SF). The base and the detail layer are superposed to construct the final fused image. Experimental results demonstrate that the proposed method can obtain state-of-the-art performance for fusion of multi-focus images.

Keywords: focus region detection, guided image filter, multi-focus image fusion

1 Introduction

Image fusion aims at synthesizing a image which is more informative for visual perception and computer processing. In recent years, multi-focus image fusion has received considerable researchers' attention for its effectiveness in overcoming the limited focus depth of the optical lens in imaging camera. Owing to this technology, one can easily obtain an image that contains all relevant objects in focus. A significant number of methods about this technology have been proposed [1-6] to get a full focus image that contains the feature information of different focused regions. These methods can be roughly classified into two groups: transform domain and spatial domain fusion [7].

Transform domain based algorithms usually transform the source images into other fields from spatial field. There are many strategies in transform domain like multi-scale transforms and others. Many kinds of multi-scale transforms have been adopted for image fusion, such as Pyramid transforms (LAP) [8], Discrete Wavelet Transform (DWT) [9-11] and Complex Wavelet Transform (CWT) [12-13]. In recent years, some image transformation methods with higher directional sensitivity than wavelets have been designed, such as Shertlet transform [14], Curvelet Transform (CVT) [15-16] and Nonsubsampled Contourlet Transform (NSCT) [17-18]. Also, some methods like Sparse Representation (SR) [19-20] are applied to image fusion. The transform domain based image fusion algorithms have achieved great success in many situations. However, the fused images of these algorithms may clutter the image content in the fusion result and suffer some global effects (e.g. visual artifacts or blurring effects).

The spatial domain based algorithms can effectively avoid the disadvantages discussed above and have received considerable researchers' attention in recent years. They be classified into three categories: pixel-based, block-based and region-based algorithms [21-22]. The main principle is to accurately detect the focused pixel or region from the source images according to some focus measures.

Until now, a variety of pixel-based image fusion algorithms have been developed, such as guided filtering based algorithm [23], multi-scale weighted gradient based algorithm [24] and SIFT [25] based algorithm. Firstly, the fusion decision map is generated from each source image by detecting the focused pixels according to the single pixel's clarity. Then, the fusion decision map is refined through some

---

* Corresponding Author

effective tools. Although these algorithms could improve the visual qualities of the fusion images, most of them might lose some useful image information due to ignore the clarity of neighbors surrounding a pixel. Besides, the rate of error identification is relative high because a single pixel cannot objectively reflect focusing property. The fused image quality is not ideal because the traditional pixel-level based multi-focus image fusion methods are less accurate and the details may be lost in the source image. The guided filtering fusion algorithm can deal with these problems, but it may generate slight fuzzy boundary.

The block-based image fusion algorithms have also been developed, such as Spatial Frequency (SF) [26], Energy of Laplacian (EOL) [27] and Sum-Modified-Laplacian (SML) operator [28]. Firstly, source images are divided into blocks with equal size. Then, the block with greater focus-measures is identified as the focus block. Finally, the fused image is filled by blocks with higher sharpness. The quality of fused images are restricted to the block size. However, the block-based method may lead to blocking artifacts of the fused image. Besides, it is difficult to determine accurately whether a pixel belongs to the focus region or not and it is easy to lose edges and detail information during the fusion.

To overcome the above issues, in this paper we propose a novel multi-focus image fusion method in spatial domain. At the beginning, to prevent the loss of essential information and the introduction of artifacts, we conduct effective filtering which not only extracts relevant image details but also reduce noise influences. Guided image filtering decomposes the input images into the base and detail layers at successive spatial scales. Then, the focus detection in the base layer is done using energy of image gradient (EOG). To correct the misjudgment on the smooth regions, block-based consistency verification is applied to generate the final decision maps. In order to improve the accuracy of the determination of the focal regions and suppress the block artifact, the focus area in the detail layer is detected using SF. Finally, to integrate the advantages of detection results of different layers, these maps are combined to produce a final decision map for each of source image. The base and the detail layer are superposed according to the final decision maps to form the fused image.

The contributions of this paper can be concluded as the following two aspects: (1) proposing a novel multi-focus image fusion algorithm based on guided image filtering; (2) The focus areas of the different layers are detected using different rules. The proposed algorithm has been tested on the commonly used image sets under three objective quality metrics. The experimental results show that the proposed method is effective by comparing with several state-of-the-art algorithms in terms of both qualitative and quantitative evaluations.

The remainder of this paper is organized as follows. Section 2 provides a detailed description of the new focus measure generated by the guided image filter. In Section 3, the method employed for detecting focused regions is shown and the proposed fusion strategy is described. Experimental results are presented in Section 4, as well as some discussions and a performance analysis. Finally, some conclusions are given in Section 5.

2 Related Work

A guided image filter [35] is a translation-variant filter based on a local linear model, which involves a guidance image G, an input image I and an output image O. In this paper, we use the input image as the guidance image. The pixel value of output image is a linear transformation of input image I, which is illustrated in the equation (1).

$$O_i = a_k G_i + b_k, \forall i \in \omega_k .$$ (1)

where ω_k is a square window of size $(2r+1) \times (2r+1)$. This local linear model ensures that O has an edge only if G has an edge, which preserve the edge information of the source image completely. The coefficients a_k and b_k can be estimated by minimizing the squared difference between O and I in the window ω_k.

$$E(a_k, b_k) = \sum_{i \in \omega_k} ((a_k G_i + b_k - I_i)^2 + \varepsilon a_k^2) .$$ (2)

where ε is a regularization parameter. The coefficients a_k and b_k can be given directly by linear regression [29] as follows:

$$a_k = \frac{\frac{1}{|\omega|}\sum_{i\in\omega_k} G_i I_i - \overline{G}_k \overline{I}_k}{\sigma_k^2 + \varepsilon} \ . \tag{3}$$

$$b_k = \overline{I}_k - a_k \overline{G}_k \ . \tag{4}$$

where σ_k and μ_k are the variance and mean of the guidance image G in ω_k respectively, $|\omega|$ is the number of pixels in ω_k, $\overline{I}_k$ and $\overline{G}_k$ are the means of I and G in ω_k respectively.

Next, the value of O_i can be calculated according to Eq.(1). A pixel i is contained in different windows ω_k. So the value of O_i in (1) equation is different when it is computed in different windows ω_k. To solve this problem, a simple strategy is to average the possible values of coefficients a_k and b_k. Then, the filtering output is computed by:

$$O_i = \frac{1}{|\omega|}\sum_{k:i\in\omega_k}(a_k G_k + b_k) \ . \tag{5}$$

$$O_i = \overline{a}G_i + \overline{b}_i \ . \tag{6}$$

where $\overline{a}_i = \frac{1}{|\omega|}\sum_{k\in\omega_i} a_k$, $\overline{b}_i = \frac{1}{|\omega|}\sum_{k\in\omega_i} b_k$.

Although the $(\overline{a}_i, \overline{b}_i)$ vary spatially, their gradients are much smaller than those of G near strong edges because they are the output of an average filter. As a result, we can still have $\nabla O \approx \overline{a}\nabla G$, meaning that abrupt intensity changes in G are still mostly preserved in O.

Equations (3), (4) and (6) give the relationship among G, I, and O and define the guided filter. The guided filter properties is similar to those of the edge preserving bilateral filter, when I serves as G. In fact, O_i in Eq. (6) can be rewritten as $O_i = \sum_j W_{ij}(G)I_j$, the weighting kernel W_{ij} only depends on G. We also have $a_k = \sum_j A_{ij}(G)I_j$ from Eq. (3). The kernel weights W_{ij} can also be expressed as:

$$W_{ij}(I) = \frac{1}{|\omega|^2}\sum_{k:(i,j)\in\omega_k}(1 + \frac{(G_i - \overline{G}_k)(G_j - \overline{G}_k)}{\sigma_k^2 + \varepsilon}) \ . \tag{7}$$

Because the sum of W_{ij} is 1, so the kernel is already normalized.

For simplicity, we use $G_{r,\varepsilon}(p,I)$ to denote guided filtering. Here, r denotes the size of filter kernel, p denotes the input image and I denotes the guidance image. In this paper, the input image and the guidance image are the same image. The guided image filtering is edge-preserving operator. Eq. (5) implies that pixel value O_i of output image at i is weighted average of neighboring pixel values. Besides image smoothing, the guided image filter is a structure-transferring filter which can be used to decompose the input images into the base and detail layers at successive spatial scales in this paper.

Fig. 1(b, c) show the base and detail layers of the input image 'Clock'. In this paper, the salient features of the base and detail layers are used to detect the focused regions and they are preserved well after layer decomposition. The base and detail layers are useful to discriminate accurately the focused regions from defocused regions.
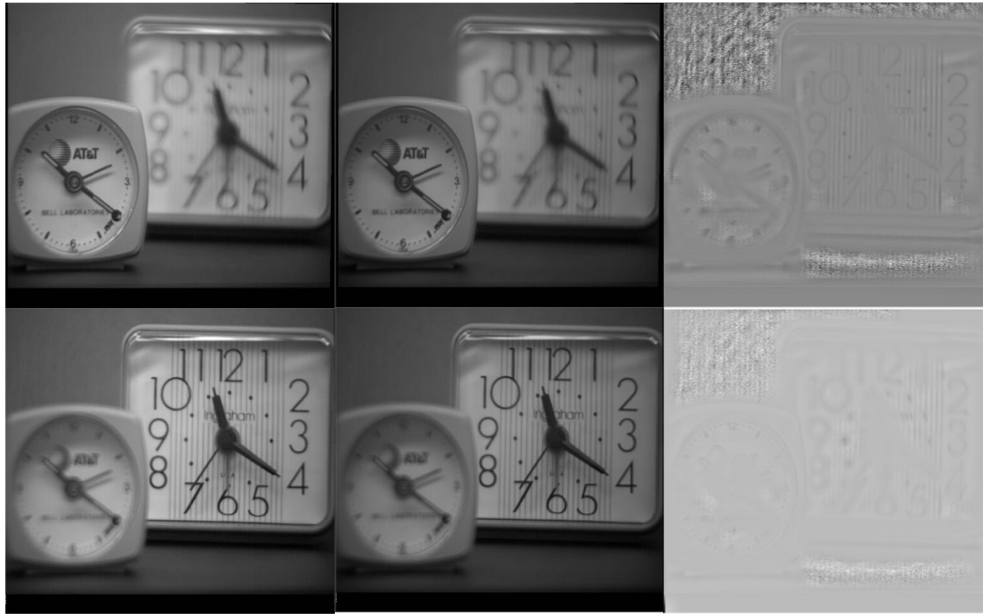
(a) Input images I (b) Base layers B (c) Detail layers D

Fig. 1. Base and detail layers decomposition results of the image "Clock" using guided filter

3 Proposed Image Fusion Method

3.1 Fusion Algorithm

In this section, a novel method guided image filtering based fusion (GFF) is proposed. A guided image filtering is used to get the two layers:the base and detail layer. The base layer contains large scale variations in intensity. The detail layer contains the small scale details. Then, the base and detail layers are fused according to certain rules. The proposed fusion framework is described in Fig. 2. The details are depicted as follows. In this paper, we assume that there are only two input source images, I_A and I_B. In fact, the proposed method can be used to fuse more than two multi-focus images. The input source images are assumed to be preregister, so the image register is not included in the framework. The fusion method contains the following 5 steps:
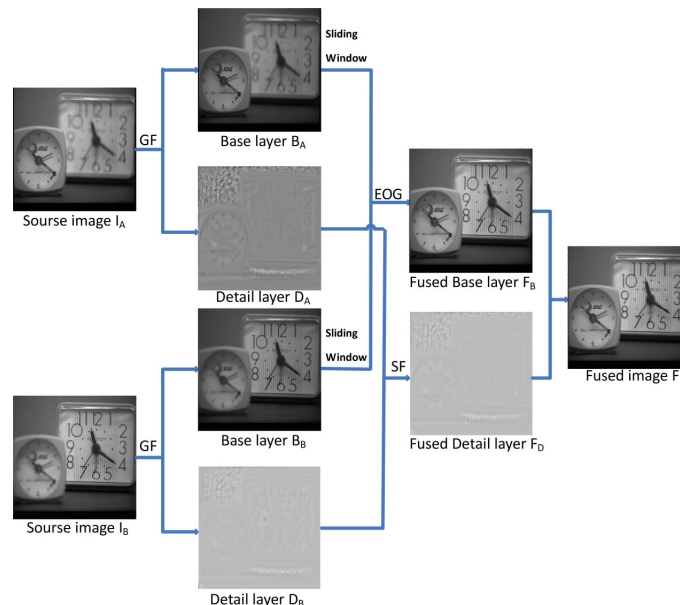

Fig. 2. Block diagram of proposed image fusion method

Step 1. Perform the guided image filtering on the input source images I_A, I_B to obtain the base and detail layer. We use B_A, D_A, B_B, D_B to denote the base and detail layer of the image I_A and I_B respectively. The base layer of the input source images is obtained as follows:

$$B_n = I_n * Z (n = A, B).$$ (8)

where I_n is the nth source image, Z is the guided image filtering. The detail layer D_n can be obtained by subtracting the base layer B_n from the source image I_n.

$$D_n = I_n - B_n (n = A, B).$$ (9)

Step 2. In the base layer of the source images, the gradient of image energy in the neighborhood of each pixel are calculated. And in the detail layer the spatial frequency are counted.

Step 3. According to the value gradient of image energy of each pixel in the neighborhood window of the base layers of two input images, we construct decision matrix H^B. And according to the value of the spatial frequency of the detail layers of two input images, decision matrix H^D is constructed.

Step 4. According to the decision matrix H^B, B_A and B_B are integrated to produce F_B which is the base layer of the fused image. Similarly, D_A and D_B are combined to form F_D which is the detail layer of the fused image.

Step 5. F_B and F_D are superposed to form the final fused image F as follows:

$$F = F_B + F_D.$$ (10)

3.2 Fusion Rule

In terms of fusion rule, there are two key issues to be solved. One is how to measure the activity level of the base and detail layer, which denotes the sharpness of the source images. We use the energy of image gradient (EOG) of the pixels to measure the activity level of the base layer. The activity level of detail layer is computed using spatial frequency. The size of the window is $(2M+1) \times (2N+1)$ and the EOG is defined as:

$$EOG(i, j) = \sum_{m=-(M-1)/2}^{(M-1)/2} \sum_{n=-(N-1)/2}^{(N-1)/2} (I_{i+m}^2 + I_{j+n}^2).$$ (11)

$$I_{i+m} = I(i + m + 1, j) - I(i + m, j).$$ (12)

$$I_{j+n} = I(i, j + n + 1) - I(i, j + n).$$ (13)

where $I(i, j)$ indicates the pixel location (i, j) in the base layer. In this paper, the size of the window is set as 7×7.

The other issue is how to produce the base layer of final fused image using base layers B_A, B_B of input images. A sliding window technique is applied to the base layer to eliminate the blocking artifacts. Let $EOG_{(i,j)}^{B_A}$ and $EOG_{(i,j)}^{B_B}$ indicate the EOG of pixel located (i, j) in B_A and B_B, respectively. Then, $EOG_{(i,j)}^{B_A}$ and $EOG_{(i,j)}^{B_B}$ are compared to determine which pixel is more likely to be classified as the focused pixel. Decision matrix H^B is constructed according to the comparison result as follows:

$$H^B(i, j) = \begin{cases} 1 & EOG_{(i,j)}^{B_A} \geq EOG_{(i,j)}^{B_B} \\ 0 & otherwise \end{cases}.$$ (14)

Where "1" in H^B means the pixel located (i, j) in image B_A is identified as focus pixel, otherwise the pixel located (i, j) in image B_B is a focus pixel.

There are some drawbacks such as thin gulfs, small holes, thin protrusions and narrow breaks in H^B,

so only by judging EOG to distinguish all the focused pixels is not sufficient. In this paper, morphological operations [30] are performed on H^B to overcome disadvantages mentioned above. Opening, denoted as $H^B \circ Z$, is simply erosion of H^B by the structure element Z. Thus thin gulfs and thin protrusions can be effectively removed. Closing, denoted as $H^B \bullet Z$, is dilation then erosion. It will conjoin narrow breaks and thin gulfs. A threshold is set to remove the holes smaller than the threshold. Thus, the final fused base layer is constructed according to the rules as follows:

$$F_B(i,j) = \begin{cases} B_A(i,j) & H^B(i,j)=1 \\ B_B(i,j) & H^B(i,j)=0 \end{cases}. \tag{15}$$

In this paper, the structure element Z of the proposed method is a 7×7 matrix with logical 1's. The threshold is set to 1000.

Spatial frequency (SF) [31] is a modified version of the EOG and it is used to measure the activity level of the detail layer. SF is defined as:

$$SF = \sqrt{(RF)^2 + (CF)^2}. \tag{16}$$

Where RF and CF are the row and column frequency respectively:

$$RF = \sqrt{\frac{1}{M \times N} \sum_{x=1}^{M} \sum_{y=2}^{N} [f(x,y) - f(x,y-1)]^2}. \tag{17}$$

$$CF = \sqrt{\frac{1}{M \times N} \sum_{x=2}^{M} \sum_{y=1}^{N} [f(x,y) - f(x-1,y)]^2}. \tag{18}$$

At the beginning, we divide the detail layer D_A and D_B into blocks [32]. Let A_i and B_i respectively indicate the ith block of D_A and D_B. Then the SF of each block is computed, and the results of A_i and B_i are denoted as M_i^A and M_i^B, respectively. Finally, compare the SF of corresponding blocks of A_i and B_i, and then construct the final detail layer of which every block is computed as follows:

$$F_{D_i} = \begin{cases} A_i, M_i^A \geq M_i^B \\ B_i, otherwise \end{cases}. \tag{19}$$

4 Experiment Results and Discussion

4.1 Experimental Settings

To verify the effectiveness of the proposed method, four pairs of multi-focus images are tested in this paper. The source images are shown in Fig. 3. The first and the second pair are gray images with size of 512×512. The third and fourth pair are gray images with size of 640×480. In general, image registration should be performed before image fusion. In this paper, the input source images are assumed to be preregistered, so image registration is not included.

Experiments are operated with Matlab R2010a in Windows environment. The computer haves Intel (R) Core (TM) i3-6100 CPU and 4G memory. To illustrate the effectiveness and superiority of the proposed method, the fusion are also performed using five state-of-the-art methods: discrete wavelet transform (DWT), laplacian pyramid (LAP), nonsubsumpled contourlet transform (NSCT), principal component analysis (PCA) and SF [33].

Specifically, the wavelet function "bi97" is used for the DWT. The decomposition levels of DWT and LAP are 4. The NSCT toolbox [36] is used for NSCT. The pyramid filter "9-7" and the orientation filter "7-9" with {4,4,3} decomposition levels are set for the NSCT. The GFF [23] is used for the proposed method. Default parameters are used in these fusion methods. In the experiment, the parameters of the fusion rule proposed in this paper are set as $r = 12$, $\varepsilon = 0.04$.

(a) are near focused image "Clock", "Pepsi", "Disk", "Lab", respectively

(b) are far focused image "Clock", "Pepsi", "Disk", "Lab", respectively

(c) are near focused image "Clock", "Pepsi", "Disk", "Lab", respectively

(d) are far focused image "Clock", "Pepsi", "Disk", "Lab", respectively

(e) are near focused image "Clock", "Pepsi", "Disk", "Lab", respectively

(f) are far focused image "Clock", "Pepsi", "Disk", "Lab", respectively

(g) are near focused image "Clock", "Pepsi", "Disk", "Lab", respectively

(h) are far focused image "Clock", "Pepsi", "Disk", "Lab", respectively

Fig. 3. Multi-focus source images

To effectively evaluate the perceptual quality of fused images, we make uses of visual comparison and quantitative evaluation. Therefore, the metrics which can validly assess the perceptual quality of fused results are commonly used. Although numerous researchers have devoted efforts in developing evaluate metrics, none of them can always objectively evaluate the perceptual quality of fused images. To solve this problem, the strategy commonly used is making an overall evaluation by combining several metrics. In this paper, three metrics are employed to assess the fusion result, which are mutual information (MI) [37], $Q^{AB/F}$ [34] and Running time respectively. MI reveals the dependence severity of the input images between the fused image. $Q^{AB/F}$ reflects the count of edge information from the input images to the fused image. For all of these metrics excepting running time, the greater values indicate the better performance.

4.2 Comparison Results

For qualitative comparison, the "Clock", "Pepsi", "Disk" and "Lab" fused images of different methods are shown in Fig. 4 to Fig. 7, respectively. The difference images between the left focused source image "Lab" and its corresponding fused images obtained by different methods are shown in Fig. 8.

In the fused images, the upper boundary of the clock in Fig. 4(a) to Fig. 4(d), the right margin of the pepsi in Fig. 5(a) to Fig. 5(d), the blurry regions of the white book in Fig. 6(a) to Fig. 6(e) and the upper edge of the student's head in Fig. 7(a) to Fig. 7(d) show the fused images obtained by the other fusion methods have artifacts and blurs, while the proposed method avoid introducing artificial textures into the fused images. The difference images show that our method is better than others in Fig. 8. It shows that the proposed algorithm has the best visual appearance and has a significant suppression of artificial texture, which is mainly due to preserving the spatial continuity by using guided filtering.

In addition, blocking artifacts obviously appear in the fused images obtained by SF, such as the upper edge of the clock in Fig. 4(e) and the disk in Fig. 6(e), the letter of the top right in Fig. 5(e) and the upper edge of the student's head in Fig. 7(e). The student's head in the fused images in Fig. 7(a) to Fig. 7(c) of DWT, LAP and NSCT show obvious misregistration. There are distortions in the difference images in Fig. 8(a) to Fig. 8(c). Misregistration is also shown in the difference image of PCA in Figs. 8(d). There are a few residuals in the right regions of Fig. 8(d) to Fig. 8(e).
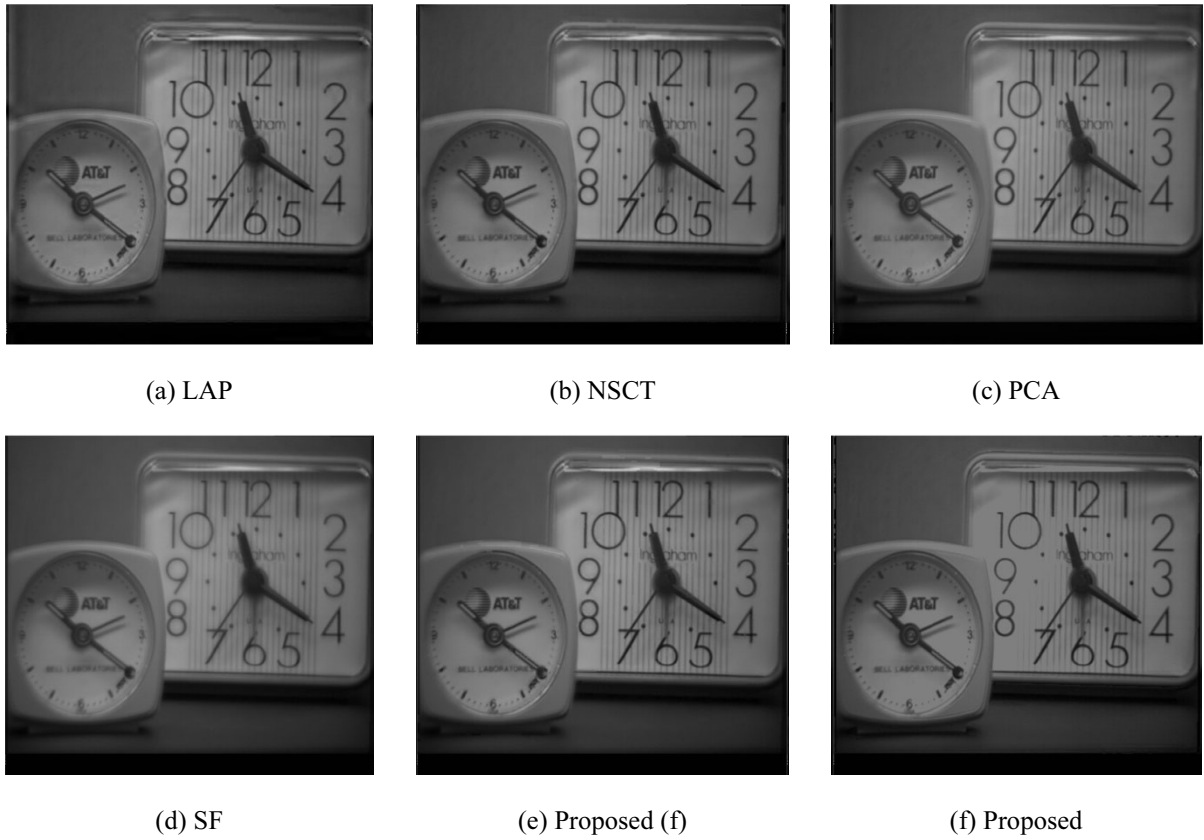
(a) LAP (b) NSCT (c) PCA

(d) SF (e) Proposed (f) (f) Proposed

Fig. 4. The fused images "Clock" obtained by DWT

(a) LAP (b) NSCT (c) PCA

(d) SF (e) Proposed (f) Proposed
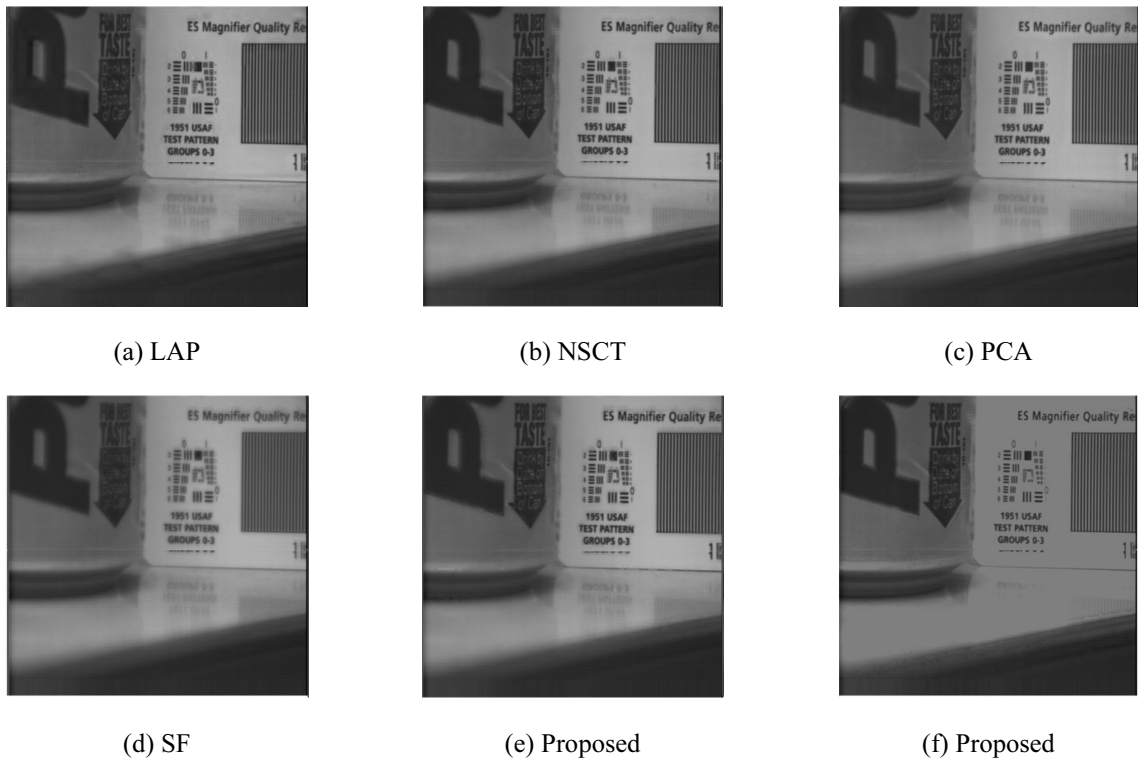
Fig. 5. The fused images "Pepsi" obtained by DWT

(a) LAP   (b) NSCT   (c) PCA

(d) SF   (e) Proposed   (f) Proposed
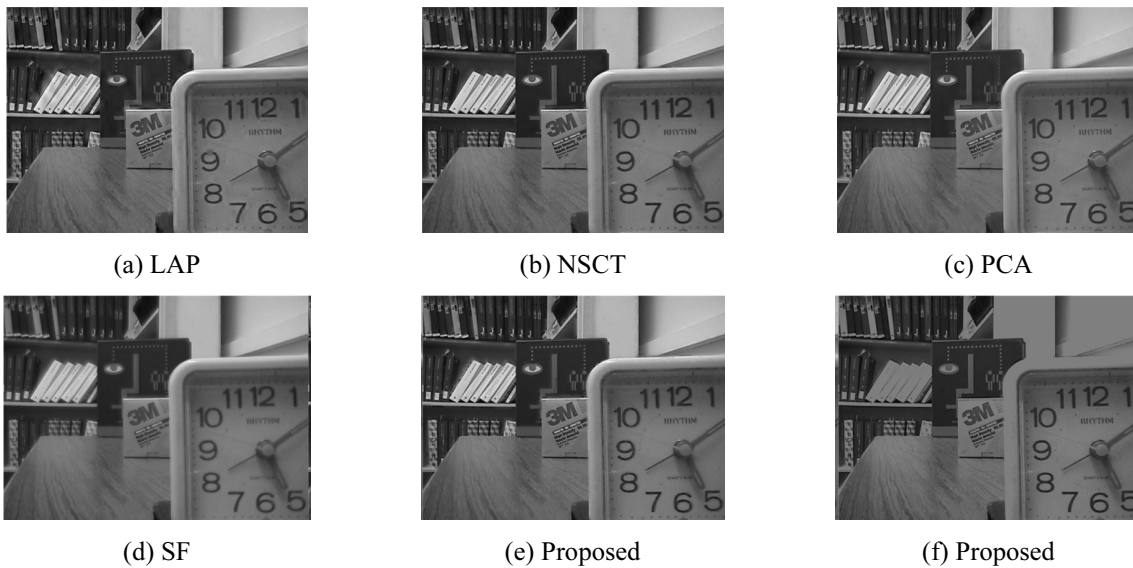
Fig. 6. The fused images "Disk" obtained by DWT

(a) LAP   (b) NSCT   (c) PCA

(d) SF   (e) Proposed   (f) Proposed
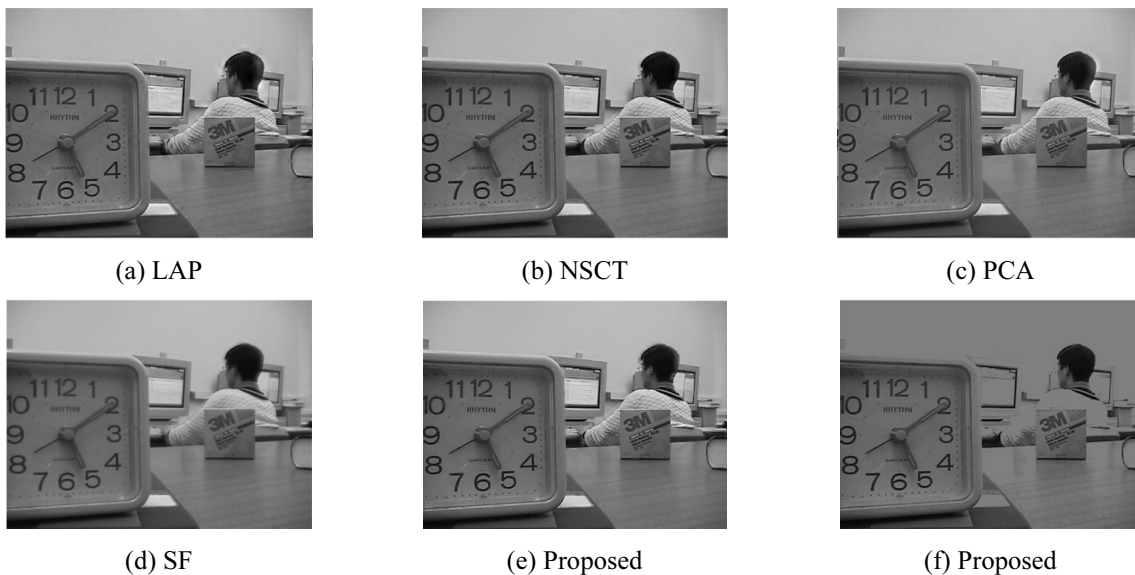
Fig. 7. The fused images "Lab" obtained by DWT

(a) LAP   (b) NSCT   (c) PCA

(d) SF   (e) Proposed   (f) Proposed
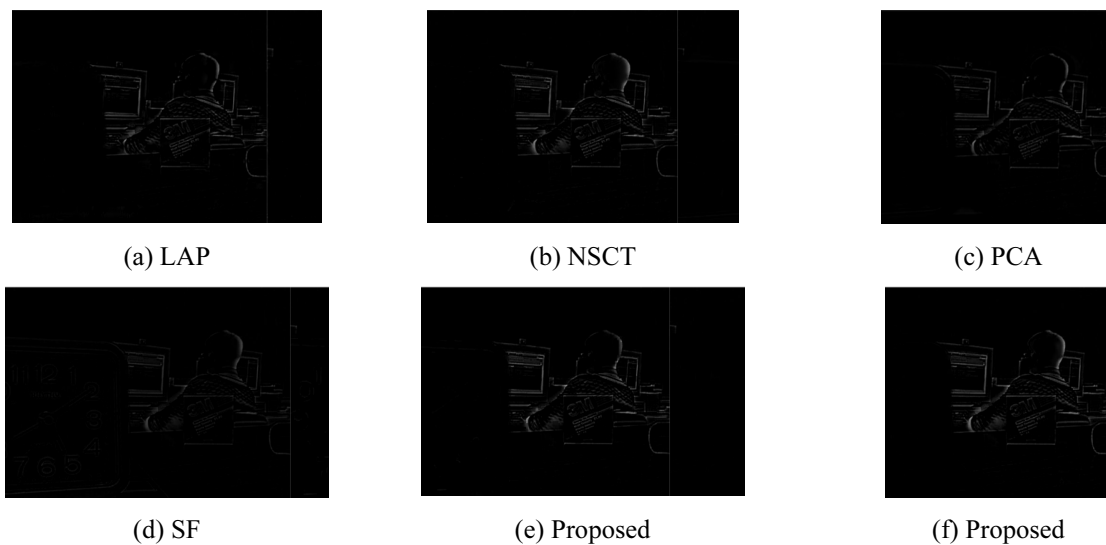
Fig. 8. The difference images between left focused source image "Lab" and corresponding fused images obtained by DWT

In this paper, the fused images obtained by PCA are worse than that of the other methods, and the fused images obtained by the proposed method are the best. There are obvious residuals in the fused images obtained by the other methods excepted the proposed method. The fused images obtained by the proposed method achieve outstanding visual performance, because it contain all the focused regions without introducing artifacts.

For quantitative comparison, the three objective criteria mentioned above are used to investigate the performance of different fusion methods. The quantitative results in three quality measures are shown in Table 1 and the histograms are also shown in Fig. 9. From Table 1, we can see that the proposed algorithm obtains higher MI and $Q^{AB/F}$ values than other methods, which respectively shows that the proposed algorithm not only improve the ability of preserving image information, but also fully retain the edge information. It is because guided filtering enhances spatial continuity which can preserve more spatial and texture information of multi-focus source images.

Table 1. The performance of different fusion methods for gray scale images

Method	clock			disk		
	MI	$Q^{AB/F}$	Running time(s)	MI	$Q^{AB/F}$	Running time(s)
LAP	6.9328	0.6872	0.3620	6.1473	0.6864	0.3949
DWT	5.8622	0.6316	0.2654	5.3572	0.6438	0.2850
NSCT	6.3199	0.6708	81.8882	5.7110	0.6707	94.4406
PCA	6.9909	0.5777	0.0097	6.0234	0.5333	0.0115
SF	7.6722	0.6768	0.2908	7.0017	0.6794	0.3564
Proposed	**7.9956**	**0.7298**	11.0099	**7.1277**	**0.7234**	12.3480

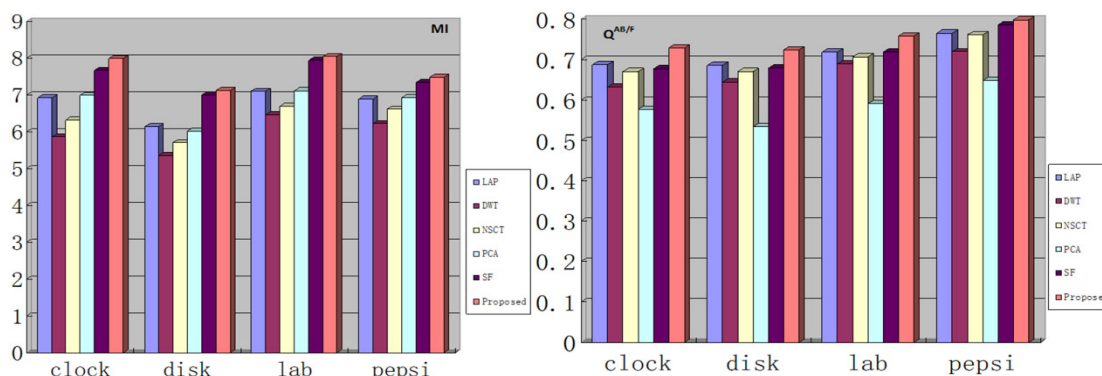| Method	lab			pepsi		
	MI	$Q^{AB/F}$	Running time(s)	MI	$Q^{AB/F}$	Running time(s)
LAP	7.1057	0.7195	0.3944	6.8937	0.7649	0.3763
DWT	6.4676	0.6896	0.2841	6.2215	0.7196	0.2825
NSCT	6.7027	0.7066	95.0865	6.6128	0.7611	84.9889
PCA	7.1224	0.5904	0.0103	6.9227	0.6477	0.0138
SF	7.9444	0.7194	0.3480	7.3440	0.7866	0.3163
Proposed	**8.0501**	**0.7586**	11.7380	**7.4843**	**0.7978**	11.0569

Fig. 9. The performance of different fusion methods for gray images

The running time of the proposed method is larger than that of the other methods except for NSCT. Because the computation of EOG of all pixels of each sliding window cost extra time.

5   Conclusions

In this paper, we proposed a novel multi-focus images fusion method. First guided image filtering is used to decompose the source images into the base and detail layer. Then, different methods are employed in different layers to detect focus regions. The proposed image fusion scheme achieves spatial consistency by using guided image filtering at the decomposition stage of the fusion. Experimental results on

different multi-focus images demonstrate that the proposed method is superior to state-of-the-art multi-focus image fusion methods in both quantitative assessments and visual effects. But the proposed method is time-consuming for the computation of total EOG. In the future, we will consider optimizing the proposed method to reduce the computational time and extending it to the fusion of color images.

Acknowledgements

References

[1] H. Li, Y. Chai, Z. Li, A new fusion scheme for multifocus images based on focused pixels detection, Machine Vision & Applications 24(6)(2013) 1167-1181.

[2] J. Wang, Q. Li, Z. Jia, N. Kasabov, J. Yang, A novel multi-focus image fusion method using PCNN in nonsubsampled contourlet transform domain, Optik- International Journal for Light and Electron Optics 126(20)(2015) 2508-2511.

[3] D. Guo, J. Yan, X. Qu, High quality multi-focus image fusion using self-similarity and depth information, Optics Communications 338(338)(2015) 138-144.

[4] B. Zhang, X. Lu, H. Pei, H. Liu, Y. Zhao, Multi-focus image fusion algorithm based on focused region extraction, Neurocomputing 174(PB)(2016) 733-748.

[5] J. Duan, G. Meng, S. Xiang, C. Pan, Multifocus image fusion via focus segmentation and region reconstruction, Neurocomputing 140(140)(2014) 193-209.

[6] Y. Yang, S. Tong, S. Huang, P. Lin, Multifocus image fusion based on NSCT and focused area detection, IEEE Sensors Journal 15(5)(2015) 2824-2838.

[7] S. Li, X. Kang, J. Hu, B. Yang, Image matting for fusion of multi-focus images in dynamic scenes, Information Fusion 14(2)(2013) 147-162.

[8] Z. Liu, K. Tsukada, K. Hanasaki, Y.K. Ho, Y.P. Dai, Image fusion by using steerable pyramid, Pattern Recognition Letters 22(9)(2001) 929-939.

[9] J. Tian, L. Chen, Adaptive multi-focus image fusion using a wavelet-based statistical sharpness measure, Signal Processing 92(9)(2012) 2137-2146.

[10] G. Pajares, J.-L. Cruz, A wavelet-based image fusion tutorial, Pattern Recognition 37(9)(2004) 1855-1872.

[11] Q. Guihong, Z. Dali, Y. Pingfan, Medical image fusion by wavelet transform modulus maxima, Optics Express 9(4)(2001) 184-190.

[12] J.J. Lewis, R.J. O'Callaghan, S.G. Nikolov, D.R. Bull, N. Canagarajah, Pixel and region based image fusion with complex wavelets, Information Fusion 8(2)(2007) 119-130.

[13] S. Ioannidou, V. Karathanassi, Investigation of the xual-free complex and shift-invariant discrete wavelet transforms on quickbird image fusion, Geoscience & Remote Sensing Letters IEEE 4(1)(2007) 166-170.

[14] Q.G. Miao, C. Shi, P.F. Xu, M. Yang, Y.B. Shi, A novel algorithm of image fusion using shearlets, Optics Communications 284(6)(2011) 1540-1547.

[15] I.M. Eldokany, A curvelet transform approach for the fusion of MR and CT images, Journal of Modern Optics 57(4)(2010) 273-286.

[16] L. Dong, Q. Yang, H. Wu, H. Xiao, M. Xu, High quality multi-spectral and panchromatic image fusion technologies based on Curvelet transform, Neurocomputing 159(C)(2015) 268-274.

[17] A.D.U. Jianhua, W. Minghui, W. Zhenya, Z. Zhongli, Multi-focus image fusion based on the non-subsampled contourlet transform, Journal of Modern Optics 59(15)(2012) 1355-1362.

[18] S.M. Darwish, Multi-level fuzzy contourlet-based image fusion for medical applications, Iet Image Processing 7(7)(2013) 694-700.

[19] C.L.P. Chen, J. Li, L. Chen, Regional multifocus image fusion using sparse representation, Optics Express 21(4)(2013) 5182-5197.

[20] Y. Liu, S. Liu, Z. Wang, A general framework for image fusion based on multi-scale transform and sparse representation, Information Fusion 24(2015) 147-164.

[21] I. De, B. Chanda, Multi-focus image fusion using a morphology-based focus measure in a quad-tree structure, Information Fusion 14(2)(2013) 136-146.

[22] B.K.S. Kumar, Image fusion based on pixel significance using cross bilateral filter, Signal Image & Video Processing 9(5)(2015) 1193-1204.

[23] S. Li, X. Kang, J. Hu, Image fusion with guided filtering, IEEE Transactions on Image Processing A Publication of the IEEE Signal Processing Society 22(7)(2013) 2864-2875.

[24] Z. Zhou, S. Li, B. Wang, Multi-scale weighted gradient-based fusion for multi-focus images, Information Fusion 20(1)(2014) 60-72.

[25] Y. Liu, S. Liu, Z. Wang, Multi-focus image fusion with dense SIFT, Information Fusion 23(3)(2015) 139-155.

[26] S. Li, B. Yang, Multifocus image fusion using region segmentation and spatial frequency, Image & Vision Computing 26(7)(2008) 971-979.

[27] M. Subbarao, T.S. Choi, A. Nikzad, Focusing techniques, Optical Engineering 32(11)(1993) 2824-2836.

[28] S.K. Nayar, Y. Nakagawa, Shape from focus, IEEE Transactions on Pattern Analysis & Machine Intelligence 16(8)(1994) 824-831.

[29] N.R. Draper, H. Smith, Applied Regression Analysis, second ed., John Wiley & Sons, New York, 1981.

[30] X. Bai, F. Zhou, B. Xue, Image enhancement using multi scale image features extracted by top-hat transform, Optics & Laser Technology 44(2)(2012) 328-336.

[31] A.M. Eskicioglu, P.S. Fisher, Image quality measures and their performance, IEEE Trans. Commun 43(12)(1995) 2959-2965.

[32] W. Huang, Z. Jing, Evaluation of focus measures in multi-focus image fusion, Pattern Recognition Letters 28(4)(2007) 493-500.

[33] S. Li, J.T. Kwok, Y. Wang, Combination of images with diverse focuses using the spatial frequency, Information Fusion 2(3)(2001) 169-176.

[34] C.S. Xydeas, V. Petrovic, Objective image fusion performance measure, Military Technical Courier 36(4)(2000) 308-309.

[35] K. He, J. Sun, X. Tang, Guided image filtering, in: Proc. European Conference on Computer Vision, 2010.

[36] J. Zhou, A.L. Cunha, M.N. Do, Nonsubsampled contourlet transform: construction and application in enhancement, in: Proc. IEEE International Conference on Image Processing, 2005.

[37] D.J.C. MacKay, Information Theory, Inference, and Learning Algorithms, Cambridge University Press, Cambridge, UK, 2003.